ACS Biomaterials SCIENCE & ENGINEERING

pubs.acs.org/journal/abseba

Letter

Codelivery Material System of Polymer Microfiber Structures for Synergistic Localized Therapy of Glioblastoma

Daewoo Han,‡ Hasan Slika,‡ Aanya Shahani, Eliana S. Wolf, Charles G. Eberhart, Henry Brem, Betty Tyler, and Andrew J. Steckl*

Cite This: https://doi.org/10.1021/acsbiomaterials.5c01482

Read Online

ACCESS | Metrics & More | Article Recommendations | Supporting Information

ABSTRACT: Glioblastoma is a highly aggressive brain tumor whose treatment has improved little over the past decade. We report on the synergistic effect of the FDA-approved anti-GBM drug (temozolomide) and inhibitors (acriflavine, PT2385) of hypoxia-inducible factors (HIFs) embedded into coaxial fiber membranes (NanoMesh). *In vitro* cytotoxicity has been evaluated for various glioma cell lines, and synergistic drug combinations have been identified. Preliminary animal studies with the three-drug-loaded NanoMesh indicate a significant improvement of median survival of >50 days and long-term (>120 days) survival rate of 40%, indicating the potential of this material platform as a translatable local GBM therapy.

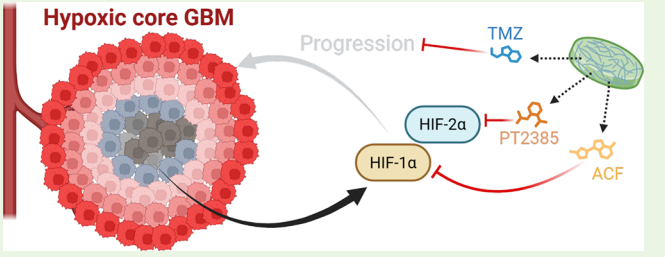

KEYWORDS: *glioblastoma, hypoxia inhibitor, local drug delivery, coaxial electrospinning, nanofiber, synergism, multiple drug therapy*

Glioblastoma (GBM) is the most common and highly aggressive primary malignant brain tumor, with a high recurrence rate over 90%, a very short median survival time of ~1.5 years, and only marginal improvement in therapeutic management over recent years.[1−3] Developing effective strategies to treat GBM is challenging due to its invasiveness, suppressive immune microenvironment, evasive stem-cell population, and marked cellular heterogeneity. Conventional treatment consists of surgical resection followed by radiation therapy and systemic chemotherapy[4] using temozolomide (TMZ). Because GBM recurrence appears within ~2 cm of the original surgical lesion, local drug delivery[5] is an effective approach to significantly reduce the recurrence rate.[6,7] The FDA-approved biodegradable wafers infused with carmustine (BCNU) (Gliadel) are implanted along the inner walls of the resection cavity created after maximal safe tumor resection.[8,9] Local delivery provides high drug concentrations in the tumor region by avoiding the challenging transport across the blood-brain barrier (BBB) that hinders the crossing of systemically-administered drugs.[10] Additionally, the BBB prevents reverse drug transport maintaining high intracranial drug concentration with minimal systemic toxicity.[11] Advances in the understanding of glioma pathogenesis and biomedical engineering have shown that the modest but significant survival benefit gained by Gliadel wafer implantation can be attributed to: (1) use of a single drug (BCNU) allows heterogeneous tumor cells to become resistant to therapy;[12−14] (2) relatively short duration of drug release leads to limited drug biodistribution into the targeted region of the brain.[5,15,16] Hence, there is a pressing need for developing novel delivery systems that can provide long-term sustained release of multiple synergistic drug candidates to augment treatment efficacy and curb tumor recurrence. Recent studies have shown that simultaneously targeting CD133 + glioma stem cells and CD133- differentiated tumor cells with minocycline and STAT3 inhibitor produces synergistic therapeutic effects and significantly limits tumor growth. This clearly presents the benefit of combination therapies to address tumor heterogeneity and resistance mechanisms.[17]

Among the types of local delivery methods and drug carriers[11,18−21] that have been investigated, electrospun fiber membranes provide unique benefits as a local chemotherapy vehicle. Electrospinning produces continuous nanofibers, with controlled diameters ranging from nanometers to micrometers.[22,23] The final product is a highly porous nonwoven nanofiber membrane. The physical and chemical properties of nanofibers can be easily manipulated by controlling various parameters, such as polymer and additive concentrations,[24] solvent/precursor selection,[25,26] electric field strength,[27] collector types,[28] etc. Moreover, the versatility of electrospinning can be significantly expanded by forming core-sheath fibers using coaxial electrospinning.[29] In addition to the intrinsic advantages of fiber electrospinning, coaxial electrospinning enables

Received: August 21, 2025
Revised: May 1, 2026
Accepted: May 4, 2026

(1) multifunctional properties by combination of two or more materials into one fiber; (2) encapsulation of multiple functional molecules into specified layers; and (3) control of their release rate by designing fiber structure, dimensions, and compositions. Previously, we demonstrated[30] that BCNU embedded in biodegradable core-sheath fibers engineered through coaxial electrospinning can provide sustained release of the BCNU drug up to 150 days along with excellent *in vivo* results in a rat brain 9L tumor model. Here, we focus on developing and testing an optimized drug delivery platform to simultaneously deliver synergistic combinations of multiple chemotherapeutic agents directly at the tumor site. For this purpose, we have developed the NanoMesh concept, which transforms as-electrospun planar thin membranes into three-dimensional tablet-like formulations suitable for surgical implantation, providing ∼2 times higher drug loading density per volume and the sustained release of the drugs embedded into the complex multilayered core-sheath fiber structure. The short- and long-term release kinetics from NanoMeshes containing single and multiple drugs can be manipulated and reliably controlled.

Innovating more effective therapeutic options for GBM requires a multifaceted approach that not only induces tumoral cell death but also targets different cellular processes and molecular pathways, underlying its aggressive behavior and treatment resistance (invasion, stemness, immune suppression, and angiogenesis). One such pathway is that mediated by hypoxia inducible factors (HIFs) as demonstrated by ample evidence in the literature.[31] The rapid growth of tumors leads to a decreased amount of oxygen being delivered to cells, producing a low-oxygen (hypoxic) environment. In turn, this triggers the activation of HIFs that enable the tumor cells to adapt to the hypoxic environment. Studies have demonstrated the significance of tumor hypoxia being associated with aggressive tumor phenotypes, which are strongly correlated with GBM stem cell phenotype, immunosuppressive microenvironment, neo-angiogenesis, and the invasive capacity of the tumor (Figure 1a), resulting in tumor recurrence, resistance to chemo/radiotherapy, and decreased survival rates.[30] Additionally, HIF-1α has been implicated in the development of treatment resistance in GBM cells against TMZ.[32,33] HIF-2α has been shown to be involved in maintaining the stemness of glioblastoma stem cells (GSCs)[34] and in promoting the immune suppressive tumor microenvironment in GBM.[35] To combat the multiple ways in which GBM can elude drug effectiveness, a multifaceted therapy including the inhibition of HIFs is desirable. Also, pro-oxidant therapeutic strategies have emerged that utilize the elevated reactive oxygen species (ROS) levels in GBM cells. The combination of doxorubicin (DOX)-induced ROS generation and photodynamic therapy (PDT) can further increase intracellular ROS levels beyond the tolerable limit, leading to the targeted death of GBM cell lines such as U87MG and T98G while being less cytotoxic to normal glial cells.[36] More recently, light-responsive hydrogels incorporating poly(3-hexylthiophene) (P3HT) nanoparticles were developed to act as both photoinitiators and photosensitizers, producing ROS upon irradiation with visible light, leading to significantly reduced glioma cell viability through localized oxidative stress.[37] In this context, several drugs inhibiting HIFs have emerged as potential anticancer medications. In particular, acriflavine, a topical antiseptic drug and a HIF-1α inhibitor, has shown promising preclinical evidence for use in brain tumor therapy.[38,39] Additionally, PT2385, a HIF-2α inhibitor, prevents the activation of downstream genes related to

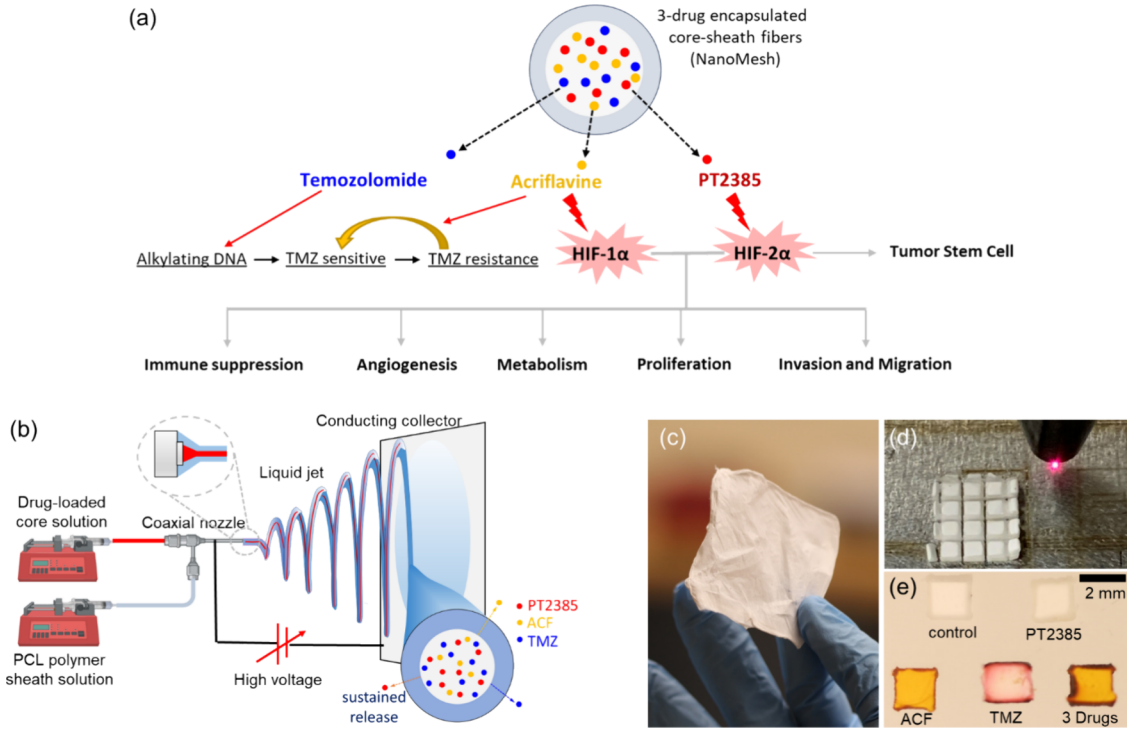

Figure 1. (a) Combined therapeutic effect of temozolomide (TMZ), an alkylating chemotherapeutic agent, and the HIF inhibitor drugs acriflavine (ACF) and PT2385. (b) NanoMesh fabrication: coaxial electrospinning for producing drug-loaded core-sheath fibers. (c) As-electrospun nanofibrous membrane. (d) CO_2 laser milling process for NanoMesh patterning after the fold-and-press densifying procedure. (e) Prepared NanoMesh samples, 2 (W) × 2 (L) × 1 (H) mm.

https://doi.org/10.1021/acsbiomaterials.5c01482
ACS Biomater. Sci. Eng. XXXX, XXX, XXX−XXX

cancer cell survival, especially for tumor stem cells.[34] TMZ, routinely used as an orally administered therapeutic in brain tumor therapy, is a DNA alkylating agent,[40] which is also effective when administered locally.

This study explores the synergistic potential between ACF, PT2385, and TMZ as a triple combination therapy against different glioblastoma cell lines and patient-derived tumor cells with heterogenous profiles. Additionally, the ability of our electrospun NanoMesh system to deliver these agents simultaneously in a controlled and sustained manner has been investigated. Finally, we have validated the translational potential of this novel therapeutic strategy by testing its long-term *in vitro* cytotoxicity and *in vivo* efficacy in reducing orthotopic tumor burden and prolonging survival in mouse models of the disease.

The basic operation of coaxial electrospinning is illustrated in Figure 1b. Solid nanofiber membranes incorporated with various drugs within a core are obtained on the collector (Figure 1c). Coaxial electrospinning parameters for all NanoMesh samples are summarized in Table S1. To obtain a 1 mm thick tablet-like 3D device, prepared coaxial fiber membranes are folded multiple times until the unpressurized thickness reaches to ∼ 2 mm (either 32 or 24 layers). Next, the folded membrane is sandwiched between two metal plates and then manually compressed using a benchtop vise grip. After densification, the membrane is attached to a metal board of a precision Universal Laser Cutter. A grid-style cut pattern was designed using the AutoCAD software. The membrane was cut into multiple small pieces of 2 mm (width) × 2 mm (length) × 1 mm (thickness) (Figure 1d) and can be easily adjusted according to resulting dimensions required. For cutting, the parameters of the laser cutter are adjusted to 15% power and 50% speed. The laser cutting process can be repeated two to three times on the same membrane if necessary. Prepared NanoMesh samples are shown in Figure 1e. This approach, in conjunction with coaxial electrospinning, significantly enhances the drug loading efficiency to nearly 100%, which is critical when costly novel drugs are incorporated. The Gliadel wafer for human use has a diameter of 14.5 mm and 1 mm thickness. For rodent intracranial implantation, smaller square tablets with a 2 to 3 mm width and 1 mm thickness are used as proof of principle.[40] The important benefit of using the laser cutting machine is the flexibility of the shape and size of the NanoMesh. For eventual human use, the size of the NanoMesh can be easily adjusted by simply changing the CAD design and parameters of laser cutting patterns.

Using coaxial electrospinning, we have produced the 3D implantable NanoMesh discs with multilayered core-sheath fibers incorporated with synergistic multiple antitumor drugs. Uniform fiber formation was obtained for no-drug control, PT2385, ACF, TMZ, and three-drug (ACF, PT2385, and TMZ) NanoMesh devices. Fiber morphologies before and after densification are shown in Figure S1. After densification, some fibers on the membrane surface were physically interfused. However, most fibers retained their as-formed fiber structure, within a less porous network. Because the membrane thickness decreased from 2 to 1 mm with almost the same apparent areas, the porosity was reduced approximately by half (from ∼80% for the as-spun membrane to ∼35−40% in the NanoMesh), and the drug loading capacity per unit volume was doubled in a NanoMesh. Since the NanoMesh is gradually hydrated from outer layers inward due to the hydrophobic fiber surface and porous fiber network, more consistent and extended-release kinetics can be obtained.

The release kinetics was measured to verify hydrophobic and hydrophilic drug release rates, as shown in Figure 2. For single-drug-loaded NanoMeshes (Figure 2a), the release rate for TMZ over the first 2 days was ∼0.28 mg/day, after which only a minimal additional amount was released (∼0.3 μg/day). ACF also showed a fast initial release of 0.18 mg/day on the first day followed by a slow continuing release of ∼1.7 μg/day for >4 weeks. The fraction of released ACF and TMZ after 24 h was ∼71 and ∼73%, respectively. The release kinetics of ACF and TMZ from the three-drug NanoMesh (Figure 2b) is similar to that in the single-drug NanoMeshes, whereas the PT2385 release kinetics was markedly different between the single and three-drug NanoMesh cases. PT2385 as a single drug was released continuously for 3 weeks, with a very slow release rate of 2.4 μg/day for 21 days and a total released amount of only ∼ 0.057 mg for 60 days. However, for the three-drug NanoMesh, the release kinetics of PT2385 indicates a sustained release profile >9 weeks with a 22× faster rate (53 μg/day) for 20 days and a ∼5× higher total amount released (0.267 mg) in 60 days. A possible explanation could be an entraining effect due to the release of the other two drugs (ACF and TMZ) in the three-drug NanoMesh, as the quicker release rates of ACF and TMZ may affect the release rate of PT2385. Both

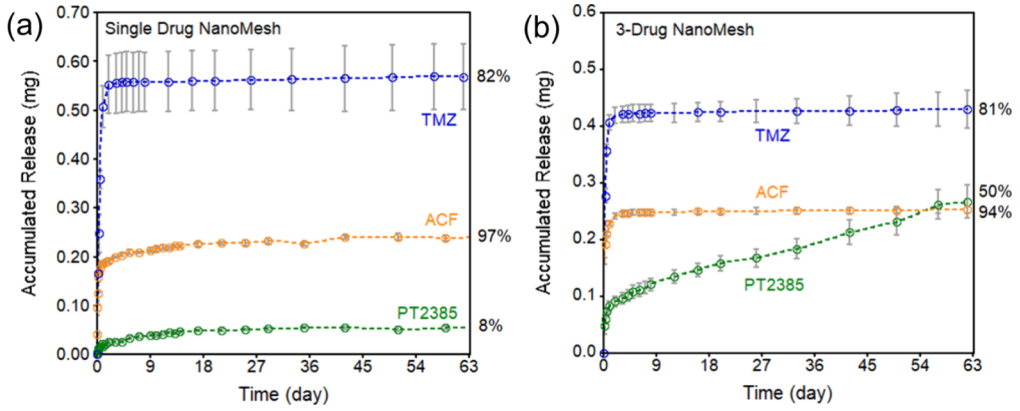

Figure 2. Drug release kinetics: (a) single-drug-incorporated NanoMesh samples and (b) all-ACF/TMZ/PT2385-incorporated NanoMesh samples (three-drug NanoMesh) ($n = 3$).

https://doi.org/10.1021/acsbiomaterials.5c01482
ACS Biomater. Sci. Eng. XXXX, XXX, XXX−XXX

ACF and TMZ presented a long-term release behavior with relatively high initial release within a day, which can be beneficial for providing the intense initial treatment followed by moderate treatment in the long-term period. However, ∼70% initial release within a day may cause local toxicity in the brain and needs to be addressed. This issue is likely due to the fiber core of coaxial fibers being exposed in places to the outer environment, leading to significant amounts of hydrophilic drugs being released.

Although the NanoMesh was successful in encapsulating and releasing all three loaded drugs, a faster release of hydrophilic ACF and TMZ drugs was observed as compared to hydrophobic PT2385. To address this issue, the trilayered coaxial electrospinning, which produces fibers with a core, an intermediate (barrier) layer, and an outer sheath structure,[42,43] can be utilized when extended long-term release of ACF and TMZ is required. In this approach, the hydrophobic intermediate layer serves as a diffusion barrier, preventing molecular transport from the fiber core to the outer sheath and ensuring that the majority of the drug remains within the core. Drug-polymer solubility and careful selection of the solvent can be optimized to generate an effective intermediate barrier layer. Another approach is to produce coaxial fibers with a noncontinuous core by employing emulsion electrospinning. In this case, oil-phase PCL solution in chloroform and the water phase of the hydrophilic drug and/or PVP in water solution can be utilized. Due to the discontinuous nature of emulsions, partial exposure of core to the wet environment will not release the significant core materials embedded with hydrophilic ACF or TMZ. Interestingly, for ACF and TMZ, their accumulated release amounts were saturated at ∼94−97% and 81−82%, respectively. Because hydrophilic drugs were mostly released from hydrophobic fiber matrix, these saturation values can be equivalent to their drug loading efficiency. While ACF has reached nearly 100% encapsulation, a relatively lower saturating percent of TMZ is possibly due to the degradation of TMZ by hydrolysis in aqueous solution. For the hydrophobic PT2385 drug, it was still continuously released until the end of the experiment. We can expect that PT2385 also has similar drug loading efficiency because all drugs were loaded in the core solution and electrospun into fibers.

To ensure a holistic approach to disease management, we investigated the synergistic potential of a HIF-1α inhibitor (ACF), HIF-2α inhibitor (PT2385), and TMZ in the context of GBM using multiple murine and human cell lines (GL261, CT2A, Mayo-39) as shown in Figure 3a. The half-maximal inhibitory concentrations (IC50) of individual drugs and the combination index (CI) of combined drugs for 97% inhibition rate were evaluated. CI < 1 represents a synergistic effect, CI > 1 is an antagonistic effect, and CI = 1 is an additive effect. Combinations of two drugs resulted in a mix of antagonistic and synergistic effects depending on the cell line. However, the three-drug combination (A + P + T) provided synergistic effects (CI values < 1) for all brain tumor cell lines. Especially, very strong synergism was presented against the MGMT-methylated cell line, one of the patient-derived xenograft (PDX) models. The evaluation of the *in vitro* synergistic long-term effects using the three-drug combination incorporated NanoMeshes is shown in Figure 3b. Results clearly demonstrate that the three-drug NanoMesh samples excelled in producing strong cytotoxicity (∼100%) for up to 28 days. To validate the biological activity of the HIF inhibitors, GL261 cells were incubated for 24 h with 10 μM of ACF and 400 μM of PT2385. Subsequently, a quantitative PCR was performed to assess the expression of *VEGF-A* and *PGK1*, which are known genes downstream of the HIF pathway for angiogenesis and cell metabolism, respectively (Figure 1a), and of *Prom1* that encodes CD133, which is a marker of GBM cell stemness. The qPCR analysis showed a significant downregulation of all three genes upon treatment. Compared to the vehicle control, ACF- and PT2385-treated samples presented a mean fold change of 0.211 ± 0.023 for *VEGF-A*, 0.057 ± 0.007 for *PGK1*, and 0.207 ± 0.025 for *Prom1* expression, corresponding to ∼79%, 95%, and 79% reduction, respectively.

In vivo efficacy testing of the drug-loaded NanoMesh was completed against orthotopic GL261 glioma tumors in mice. The GL261 model is a widely used and verified model that recapitulates the aggressiveness and treatment resistance of GBM tumors.[44] The group that received the three-drug-loaded NanoMesh had significantly increased overall survival (p value = 0.002) (Figure 4a), with 40% of the mice showing long-term survival (>120 days). Bioluminescence-based IVIS imaging (Figure 4b) clearly shows the evidence of inhibiting and clearing the tumor in mice with three-drug NanoMesh implantation, while tumors have grown quickly in the blank NanoMesh case. Tumor burden was quantified by measuring the bioluminescence intensity emitted from the GL261-luc glioma cell line as shown in Figure 4c. The graph shows that both groups started at the same average tumor burden, which

(a)

Drug	Cell lines		
	GL261	MGMT-methylated (Mayo-39)	CT2A
IC50 concentration (μM)			
ACF (A)	1.17	0.50	3.24
PT2385 (P)	331	651	1,021
TMZ (T)	4,154	1,307	1,424
Combination index (CI) at fraction killed of 97%			
T + P	2.04	0.71	3.4
T + A	0.80	0.77	4.7
A + P	1.85	0.26	0.11
A + P + T	0.83	0.14	0.76

(b)

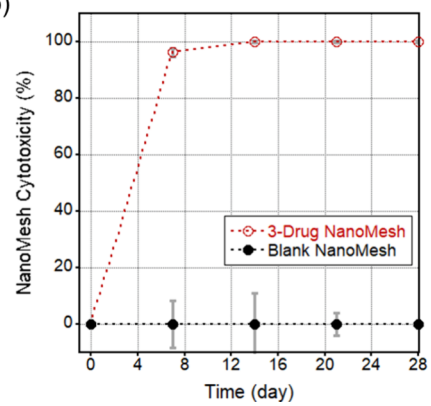

Figure 3. *In vitro* results with GBM cells: (a) cytotoxicity and synergism of ACF, PT2385, and TMZ against different GBM cell lines and (b) long-term efficacy of three-drug NanoMesh samples against the GL261 glioma cell line (n = 3).

https://doi.org/10.1021/acsbiomaterials.5c01482
ACS Biomater. Sci. Eng. XXXX, XXX, XXX−XXX

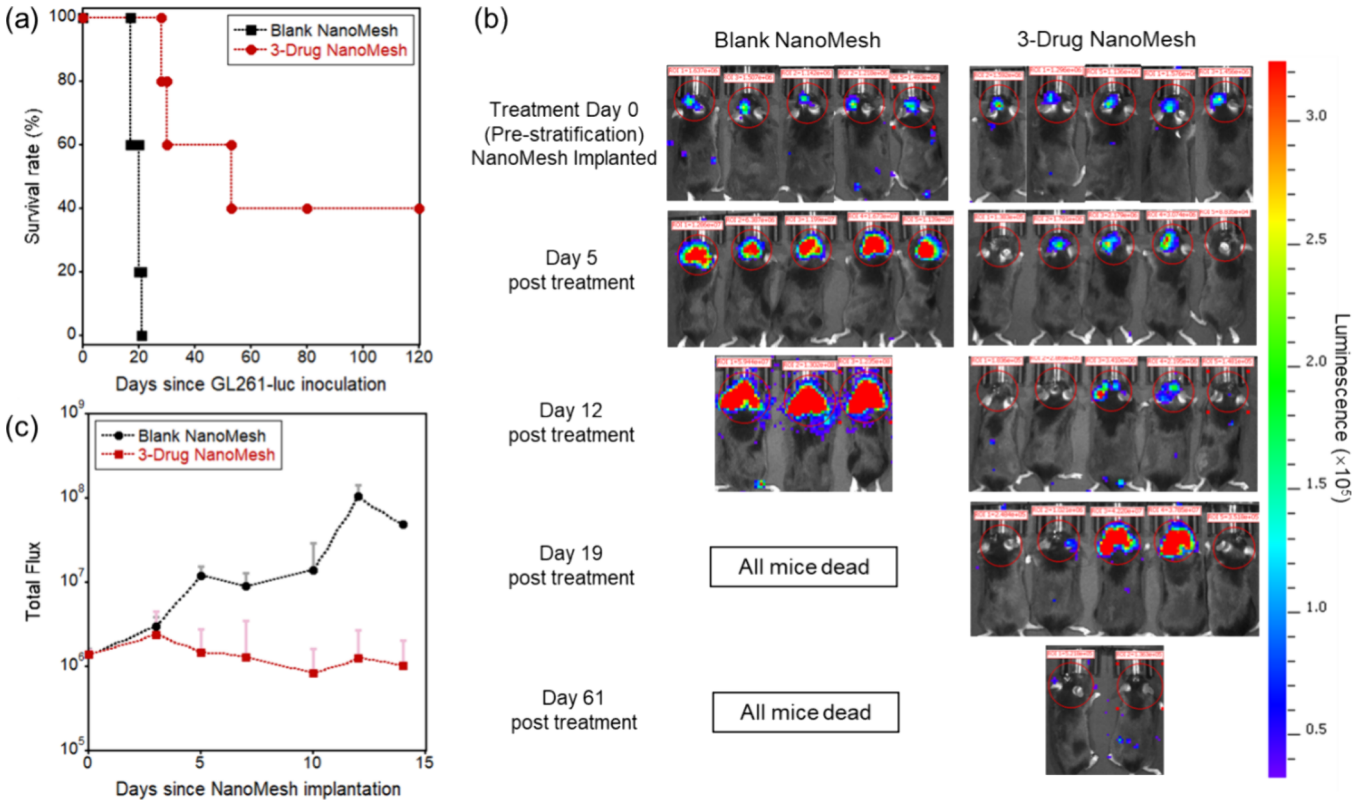

Figure 4. *In vivo* efficacy of intracranially implanted NanoMesh loaded with the three-drug combination. (a) Survival rate of C57BL6 mice implanted with orthotopic GL261 tumors and treated with either a blank NanoMesh or three-drug NanoMesh; the *p*value for the log-rank test is 0.002. (b) Bioluminescence *in vivo* imaging of the tumor burden for mice at different timepoints. (c) Quantification of the average bioluminescence emitted from mice over the first 15 days after NanoMesh implantation. NanoMesh implantation (treatment day 0) took place 7 days after tumor implantation.

progressed dramatically over the following 2 weeks in the control (blank NanoMesh) mice until they were all dead at day 14 following treatment (day 21 following tumor implantation). However, the average tumor burden remained almost constant in the three-drug NanoMesh group over this period of time. To assess the safety profile of the NanoMesh implants, the brains of a mouse from the control (blank) group and two mice from the three-drug group (one that died on day 30 and one long-term survivor that was euthanized on day 150) were harvested, fixed in formalin, embedded in paraffin, sectioned, and stained with hematoxylin and eosin by the Oncology Tissue Services core at the Johns Hopkins University. The stained slides (Figure S2) were assessed by an experienced neuropathologist (C.G.E.) who noted the absence of large hemorrhages, edema, necrosis, or inflammation in the brain parenchyma. Mild, patchy gliosis and microglial activation were noted but were equivalent in the brain implanted with the blank NanoMesh and those implanted with the three-drug NanoMesh. Scattered "red neurons" (eosinophilic neurons) morphologically suggestive of ischemic neuronal change was observed, including the hippocampus and cortex away from the lesion. These neurons were equally present in the blank and three-drug-treated tumor-bearing mice, suggesting that the changes could be related to the mass effect from the tumors. Notably, the brain of the mouse that received the three-drug NanoMesh, achieving tumor clearance and long term survival (120 days), had a higher abundance of these ischemic neurons, perhaps due to long-term exposure to the three-drug NanoMesh treatment. Nevertheless, despite this finding, no behavioral deficits were noted in any of the mice that survived long term. Furthermore, the efficacy of the three-drug NanoMesh was validated in a different more aggressive glioma model using C57BL6 mice implanted orthotopically with CT2A mouse glioma. The three-drug group clearly showed an improvement in overall survival (log-rank test p value = 0.031) as compared to the blank NanoMesh group, while all other single-drug monotherapy groups failed to show any survival benefit in this highly aggressive model (Figure S3).

In summary, synergistic drug combinations of ACF, TMZ, and PT2385 have been developed to prevent treatment resistance in GBM and improve treatment outcomes by inhibiting HIFs related to multiple downstream cascades for GBM progression. Significant amounts (~44% of NanoMesh weight) of three drugs were successfully encapsulated into nanofibers using coaxial electrospinning for controlled release. The synergistic anticancer effect of ACF, TMZ, and PT2385 against various cell lines such as GL261, Mayo-39, and CT2A has been demonstrated *in vitro*. Coaxial fibers embedded with this synergistic combination provided significant long-term *in vitro* cytotoxicity of GL261 glioma cells. Additionally, our previous work[42] has demonstrated that coaxial fibers embedded with ACF have the ability to reduce the expression of target genes downstream of HIF-1 in GL261 cells. Correspondingly, we investigated the *in vivo* efficacy of the three-drug-loaded NanoMesh in a reliable mouse model of GBM, which presented encouraging results, with 40% long-term survival. The studies indicate the potential translatability of the developed multifaceted

https://doi.org/10.1021/acsbiomaterials.5c01482
ACS Biomater. Sci. Eng. XXXX, XXX, XXX–XXX

local delivery strategy. Based on the promising results of local delivery of synergistic anti-GBM drugs, further improvements on release kinetics especially on hydrophilic drugs (ACF and TMZ) and more thorough *in vivo* evaluations will be pursued, which can significantly enhance the survival and quality of life for patients with GBM.

■ ASSOCIATED CONTENT

Supporting Information

The Supporting Information is available free of charge at https://pubs.acs.org/doi/10.1021/acsbiomaterials.5c01482.

Additional experimental details, materials and methods, including photographs of fiber membranes and brain slides (DOCX)

■ AUTHOR INFORMATION

Corresponding Author

Andrew J. Steckl – *Nanoelectronics Laboratory, Department of Electrical and Computer Engineering, University of Cincinnati, Cincinnati, Ohio 45221, United States; Department of Biomedical Engineering, University of Cincinnati, Cincinnati, Ohio 45221, United States;* orcid.org/0000-0002-1868-4442; Email: a.steckl@uc.edu

Authors

Daewoo Han – *Nanoelectronics Laboratory, Department of Electrical and Computer Engineering, University of Cincinnati, Cincinnati, Ohio 45221, United States*

Hasan Slika – *Hunterian Neurosurgical Laboratory, Department of Neurosurgery, School of Medicine, Johns Hopkins University, Baltimore, Maryland 21287, United States;* orcid.org/0000-0003-4597-3642

Aanya Shahani – *Hunterian Neurosurgical Laboratory, Department of Neurosurgery, School of Medicine, Johns Hopkins University, Baltimore, Maryland 21287, United States*

Eliana S. Wolf – *Hunterian Neurosurgical Laboratory, Department of Neurosurgery, School of Medicine, Johns Hopkins University, Baltimore, Maryland 21287, United States*

Charles G. Eberhart – *Department of Pathology, School of Medicine, Johns Hopkins University, Baltimore, Maryland 21205, United States*

Henry Brem – *Hunterian Neurosurgical Laboratory, Department of Neurosurgery, School of Medicine, Johns Hopkins University, Baltimore, Maryland 21287, United States; Departments of Oncology, Ophthalmology, and Biomedical Engineering, Johns Hopkins University, Baltimore, Maryland 21287, United States*

Betty Tyler – *Hunterian Neurosurgical Laboratory, Department of Neurosurgery, School of Medicine, Johns Hopkins University, Baltimore, Maryland 21287, United States;* orcid.org/0000-0001-9800-6969

Complete contact information is available at: https://pubs.acs.org/doi/10.1021/acsbiomaterials.5c01482

Author Contributions

‡D.H. and H.S. contributed equally. The manuscript was written through contributions of all authors. All authors have given approval of the final version of the manuscript.

Funding

This research was funded in part by NIH grant R15CA252987.

Notes

All studies involving animals were approved by the Johns Hopkins University Animal Care and Use Committee (Protocol number: MO24M346).

The authors declare no competing financial interest.

■ ACKNOWLEDGMENTS

Two authors (H.B. and B.T.) thank The Reza Khatib MD Brain Tumor Center, The Florence D. and Irving J. Sherman MD Charitable Foundation Trust, and The Venable Foundation for their philanthropic support of the Hunterian Neurosurgical Laboratory.

■ REFERENCES

(1) Stupp, R.; Hegi, M. E.; Mason, W. P.; van den Bent, M. J.; Taphoorn, M. J. B.; Janzer, R. C.; Ludwin, S. K.; Allgeier, A.; Fisher, B.; Belanger, K.; Hau, P.; Brandes, A. A.; Gijtenbeek, J.; Marosi, C.; Vecht, C. J.; Mokhtari, K.; Wesseling, P.; Villa, S.; Eisenhauer, E.; Gorlia, T.; Weller, M.; Lacombe, D.; Cairncross, J. G.; Mirimanoff, R.-O. Effects of radiotherapy with concomitant and adjuvant temozolomide versus radiotherapy alone on survival in glioblastoma in a randomised phase III study: 5-year analysis of the EORTC-NCIC trial. *Lancet Oncol.* **2009**, *10* (5), 459–466.

(2) Stupp, R.; Mason, W. P.; van den Bent, M. J.; Weller, M.; Fisher, B.; Taphoorn, M. J. B.; Belanger, K.; Brandes, A. A.; Marosi, C.; Bogdahn, U.; Curschmann, J.; Janzer, R. C.; Ludwin, S. K.; Gorlia, T.; Allgeier, A.; Lacombe, D.; Cairncross, J. G.; Eisenhauer, E.; Mirimanoff, R. O. Radiotherapy plus Concomitant and Adjuvant Temozolomide for Glioblastoma. *N. Engl. J. Med.* **2005**, *352* (10), 987–996.

(3) Bastiancich, C.; Malfanti, A.; Préat, V.; Rahman, R. Rationally designed drug delivery systems for the local treatment of resected glioblastoma. *Adv. Drug Delivery Rev.* **2021**, *177*, No. 113951.

(4) Ashby, L. S.; Ryken, T. C. Management of malignant glioma: steady progress with multimodal approaches. *Neurosurg. Focus* **2006**, *20* (4), No. E3.

(5) van Solinge, T. S.; Nieland, L.; Chiocca, E. A.; Broekman, M. L. D. Advances in local therapy for glioblastoma - taking the fight to the tumour. *Nat. Rev. Neurol.* **2022**, *18* (4), 221–236.

(6) Giese, A.; Bjerkvig, R.; Berens, M. E.; Westphal, M. Cost of Migration: Invasion of Malignant Gliomas and Implications for Treatment. *J. Clin. Oncol.* **2003**, *21* (8), 1624–1636.

(7) Weller, M.; Cloughesy, T.; Perry, J. R.; Wick, W. Standards of care for treatment of recurrent glioblastoma—are we there yet? *Neuro-Oncology* **2013**, *15* (1), 4–27.

(8) Sipos, E. P.; Tyler, B.; Piantadosi, S.; Burger, P. C.; Brem, H. Optimizing interstitial delivery of BCNU from controlled release polymers for the treatment of brain tumors. *Cancer Chemother. Pharmacol.* **1997**, *39* (5), 383–389.

(9) Lesniak, M. S.; Brem, H. Targeted therapy for brain tumours. *Nat. Rev. Drug Discovery* **2004**, *3* (6), 499–508.

(10) Affronti, M. L.; Heery, C. R.; Herndon, J. E.; Rich, J. N.; Reardon, D. A.; Desjardins, A.; Vredenburgh, J. J.; Friedman, A. H.; Bigner, D. D.; Friedman, H. S. Overall survival of newly diagnosed glioblastoma patients receiving carmustine wafers followed by radiation and concurrent temozolomide plus rotational multiagent chemotherapy. *Cancer* **2009**, *115* (15), 3501–3511.

(11) Katz, J. S.; Slika, H.; Sattari, S. A.; Malla, A. P.; Xia, Y.; Antar, A.; Ran, K.; Tyler, B. Overcoming the Blood-Brain Barrier for Drug Delivery to the Brain. *ACS Omega* **2025**, *10*, 32544–32563.

(12) Li, K. W.; Dang, W.; Tyler, B. M.; Troiano, G.; Tihan, T.; Brem, H.; Walter, K. A. Polilactofate microspheres for Paclitaxel delivery to

central nervous system malignancies. *Clin. Cancer Res.* **2003**, *9* (9), 3441–3447.
(13) Alomari, S.; Zhang, I.; Hernandez, A.; Kraft, C. Y.; Raj, D.; Kedda, J.; Tyler, B. Drug Repurposing for Glioblastoma and Current Advances in Drug Delivery-A Comprehensive Review of the Literature. *Biomolecules* **2021**, *11* (12), 1870.
(14) Hersh, A. M.; Gaitsch, H.; Alomari, S.; Lubelski, D.; Tyler, B. M. Molecular Pathways and Genomic Landscape of Glioblastoma Stem Cells: Opportunities for Targeted Therapy. *Cancers* **2022**, *14* (15), 3743.
(15) Bos, E. M.; Binda, E.; Verploegh, I. S. C.; Wembacher, E.; Hoefnagel, D.; Balvers, R. K.; Korporaal, A. L.; Conidi, A.; Warnert, E. A. H.; Trivieri, N.; Visioli, A.; Zaccarini, P.; Caiola, L.; van Wijck, R.; van der Spek, P.; Huylebroeck, D.; Leenstra, S.; Lamfers, M. L. M.; Ram, Z.; Westphal, M.; Noske, D.; Legnani, F.; DiMeco, F.; Vescovi, A. L.; Dirven, C. M. F. Local delivery of hrBMP4 as an anticancer therapy in patients with recurrent glioblastoma: a first-in-human phase 1 dose escalation trial. *Mol. Cancer* **2023**, *22* (1), 129.
(16) Chen, H.; Hu, G.; Ouyang, D. A numerical study of the distribution of chemotherapeutic drug carmustine in brain glioblastoma. *Drug Delivery Transl. Res.* **2022**, *12* (7), 1697–1710.
(17) Ohnishi, T.; Yamashita, D.; Inoue, A.; Suehiro, S.; Ohue, S.; Kunieda, T. Is Interstitial Chemotherapy with Carmustine (BCNU) Wafers Effective against Local Recurrence of Glioblastoma? A Pharmacokinetic Study by Measurement of BCNU in the Tumor Resection Cavity. *Brain Sci.* **2022**, *12*, 567.
(18) Chang, C.-H.; Liu, W.-T.; Hung, H.-C.; Gean, C.-Y.; Tsai, H.-M.; Su, C.-L.; Gean, P.-W. Synergistic inhibition of tumor growth by combination treatment with drugs against different subpopulations of glioblastoma cells. *BMC Cancer* **2017**, *17* (1), 905.
(19) Pradilla, G.; Wang, P. P.; Gabikian, P.; Li, K.; Magee, C. A.; Walter, K. A.; Brem, H. Local Intracerebral Administration of Paclitaxel with the Paclimer® Delivery System: Toxicity Study in a Canine Model. *J. Neuro-Oncol.* **2006**, *76* (2), 131–138.
(20) Tyler, B.; Fowers, K. D.; Li, K. W.; Recinos, V. R.; Caplan, J. M.; Hdeib, A.; Grossman, R.; Basaldella, L.; Bekelis, K.; Pradilla, G.; Legnani, F.; Brem, H. A thermal gel depot for local delivery of paclitaxel to treat experimental brain tumors in rats. *J. Neurosurg.* **2010**, *113* (2), 210–217.
(21) Slika, H.; Shahani, A.; Gattu, K.; Mundrathi, V.; Solan, A. A.; Gonzalez, B.; Haque, T. N.; Rahman, S.; Sugandhi, V. V.; Lee, J.; Velarde, E.; Alomari, S.; Pacis, V. L.; Brem, H.; Tyler, B.; Xin, X.; Cho, H. Intracranial Nanogel Pellets Carrying Temozolomide and Paclitaxel for Adjuvant Brain Cancer Therapy. *Mol. Pharm.* **2025**, *22* (1), 131–141.
(22) Wang, M.; Bergès, R.; Malfanti, A.; Préat, V.; Bastiancich, C. Local delivery of doxorubicin prodrug via lipid nanocapsule−based hydrogel for the treatment of glioblastoma. *Drug Delivery Transl. Res.* **2024**, *14* (12), 3322–3338.
(23) Xue, J.; Xie, J.; Liu, W.; Xia, Y. Electrospun Nanofibers: New Concepts, Materials, and Applications. *Acc. Chem. Res.* **2017**, *50* (8), 1976–1987.
(24) Schiffman, J. D.; Schauer, C. L. A Review: Electrospinning of Biopolymer Nanofibers and their Applications. *Polym. Rev.* **2008**, *48* (2), 317–352.
(25) Garcia, J.; Felix, M.; Cordobés, F.; Guerrero, A. Effect of solvent and additives on the electrospinnability of BSA solutions. *Colloids Surf., B* **2022**, *217*, No. 112683.
(26) Kern, J.; Venkatram, S.; Banerjee, M.; Brettmann, B.; Ramprasad, R. Solvent selection for polymers enabled by generalized chemical fingerprinting and machine learning. *Phys. Chem. Chem. Phys.* **2022**, *24* (43), 26547–26555.
(27) Rathore, P.; Schiffman, J. D. Effect of pH Value on the Electrical Properties of PEDOT:PSS-Based Fiber Mats. *ACS Eng. Au* **2023**, *3* (6), 527–536.
(28) Gupta, A.; Ayithapu, P.; Singhal, R. Study of the electric field distribution of various electrospinning geometries and its effect on the resultant nanofibers using finite element simulation. *Chem. Eng. Sci.* **2021**, *235*, 116463.
(29) Nadaf, A.; Gupta, A.; Hasan, N.; Fauziya; Ahmad, S.; Kesharwani, P.; Ahmad, F. J. Recent update on electrospinning and electrospun nanofibers: current trends and their applications. *RSC Adv.* **2022**, *12* (37), 23808–23828.
(30) Han, D.; Steckl, A. J. Coaxial Electrospinning Formation of Complex Polymer Fibers and their Applications. *ChemPlusChem* **2019**, *84* (10), 1453–1497.
(31) Han, D.; Serra, R.; Gorelick, N.; Fatima, U.; Eberhart, C. G.; Brem, H.; Tyler, B.; Steckl, A. J. Multi-layered core-sheath fiber membranes for controlled drug release in the local treatment of brain tumor. *Sci. Rep.* **2019**, *9* (1), 17936.
(32) Bou-Gharios, J.; Noël, G.; Burckel, H. The neglected burden of chronic hypoxia on the resistance of glioblastoma multiforme to first-line therapies. *BMC Biol.* **2024**, *22* (1), 278.
(33) Wang, P.; Gong, S.; Liao, B.; Liu, J.; Zhao, L.; Wu, N. HIF-1alpha and HIF-2alpha: synergistic regulation of glioblastoma malignant progression during hypoxia and apparent chemosensitization in response to hyperbaric oxygen. *Cancer Cell Int.* **2025**, *25* (1), 251.
(34) Lo Dico, A.; Martelli, C.; Diceglie, C.; Lucignani, G.; Ottobrini, L. Hypoxia-Inducible Factor-1alpha Activity as a Switch for Glioblastoma Responsiveness to Temozolomide. *Front. Oncol.* **2018**, *8*, 249.
(35) Renfrow, J. J.; Soike, M. H.; West, J. L.; Ramkissoon, S. H.; Metheny-Barlow, L.; Mott, R. T.; Kittel, C. A.; D'Agostino, R. B.; Tatter, S. B.; Laxton, A. W.; Frenkel, M. B.; Hawkins, G. A.; Herpai, D.; Sanders, S.; Sarkaria, J. N.; Lesser, G. J.; Debinski, W.; Strowd, R. E. Attenuating hypoxia driven malignant behavior in glioblastoma with a novel hypoxia-inducible factor 2 alpha inhibitor. *Sci. Rep.* **2020**, *10* (1), No. 15195.
(36) Espinoza, F. I.; Tankov, S.; Chliate, S.; Pereira Couto, J.; Marinari, E.; Vermeil, T.; Lecoultre, M.; El Harane, N.; Dutoit, V.; Migliorini, D.; Walker, P. R. Targeting HIF-2alpha in glioblastoma reshapes the immune infiltrate and enhances response to immune checkpoint blockade. *Cell. Mol. Life Sci.* **2025**, *82* (1), 119.
(37) Cesca, B. A.; Caverzan, M. D.; Lamberti, M. J.; Ibarra, L. E. Enhancing Therapeutic Approaches in Glioblastoma with Pro-Oxidant Treatments and Synergistic Combinations: In Vitro Experience of Doxorubicin and Photodynamic Therapy. *Int. J. Mol. Sci.* **2024**, *25* (14), 7525.
(38) Abalos, R. N.; Aziz, I. A.; Caverzan, M.; Lochedino, A. S.; Ibarra, L. E.; Gallastegui, A.; Chesta, C. A.; Gómez, M. L.; Mecerreyes, D.; Palacios, R. E.; Criado-Gonzalez, M. Poly(3-hexylthiophene) nanoparticles as visible-light photoinitiators and photosensitizers in 3D printable acrylic hydrogels for photodynamic therapies. *Mater. Horiz.* **2025**, *12* (8), 2524–2534.
(39) Mangraviti, A.; Raghavan, T.; Volpin, F.; Skuli, N.; Gullotti, D.; Zhou, J.; Asnaghi, L.; Sankey, E.; Liu, A.; Wang, Y.; Lee, D.-H.; Gorelick, N.; Serra, R.; Peters, M.; Schriefer, D.; Delaspre, F.; Rodriguez, F. J.; Eberhart, C. G.; Brem, H.; Olivi, A.; Tyler, B. HIF-1α-Targeting Acriflavine Provides Long Term Survival and Radiological Tumor Response in Brain Cancer Therapy. *Sci. Rep.* **2017**, *7* (1), 14978.
(40) Serra, R.; Mangraviti, A.; Gorelick, N. L.; Shapira-Furman, T.; Alomari, S.; Cecia, A.; Darjee, N.; Brem, H.; Rottenberg, Y.; Domb, A. J.; Tyler, B. Combined intracranial Acriflavine, temozolomide and radiation extends survival in a rat glioma model. *Eur. J. Pharm. Biopharm.* **2022**, *170*, 179–186.
(41) Ward, S. M.; Skinner, M.; Saha, B.; Emrick, T. Polymer−Temozolomide Conjugates as Therapeutics for Treating Glioblastoma. *Mol. Pharm.* **2018**, *15*, 5263–5276.
(42) Han, D.; Sherman, S.; Filocamo, S.; Steckl, A. J. Long-term antimicrobial effect of nisin released from electrospun triaxial fiber membranes. *Acta Biomater.* **2017**, *53*, 242–249.
(43) Han, D.; Steckl, A. J. Triaxial electrospun nanofiber membranes for controlled dual release of functional molecules. *ACS Appl. Mater. Interfaces.* **2013**, *5* (16), 8241–8245.
(44) Slika, H.; Karimov, Z.; Alimonti, P.; Abou-Mrad, T.; De Fazio, E.; Alomari, S.; Tyler, B. Preclinical Models and Technologies in Glioblastoma Research: Evolution, Current State, and Future Avenues. *Int. J. Mol. Sci.* **2023**, *24* (22), No. 16316.

https://doi.org/10.1021/acsbiomaterials.5c01482
ACS Biomater. Sci. Eng. XXXX, XXX, XXX−XXX